79-4052

Flight Results on Structural Dynamics from Hermes

S.C. Garg* and P.C. Hughes†
University of Toronto, Toronto, Ontario, Canada
and
R.A. Millar‡ and F.R. Vigneron§
Department of Communications, Ottawa, Ontario, Canada

Hermes is a geostationary communications satellite equipped with large flexible solar arrays instrumented for experimental purposes. A program for obtaining flight data on structural dynamics was part of the mission, including special in-flight experiments. This paper describes the design of these experiments, the instrumentation, experimental results, and related observations during array deployment and ground tests. Flight results were obtained on natural frequencies, damping factors, and steady-state resonant amplitudes. Finally, comparisons with a theoretical model are given. Generally, excellent agreement was found between measurments and predicted values. However, damping factors measured were higher than expected from ground tests.

Nomenclature

a	= acceleration, in g units
A	= amplitude of excitation or of response
B, B'	= out-of-plane, in-plane boom bending stiffness
d_n	= gain in acceleration transfer function
$f(t)$	= special excitation input waveform
F	= thrust level of attitude control jets
h_n	= integral of mode shapes
I_2	= pitch moment of inertia
k_l, k_l'	= out-of-plane, in-plane boom root spring stiffness
k_n	= gain in attitude transfer function
l	= moment arm of thruster to mass center
N	= maximum number of pulses fired
$q(t)$	= generalized coordinate in modal expansion
s	= Laplace transform variable
t, T	= time, time of response output
T_2	= pitch torque on center body
v	= deflection of flexible blanket
x, y, z	= spatial coordinates
$\alpha_n(y)$	= twist mode shape
γ	= array angle (see Fig. 1)
δ	= $\phi\cos\gamma - \psi\sin\gamma$
ϵ	= $\phi\sin\gamma + \psi\cos\gamma$
Δ	= excitation pulse width
ζ	= equivalent viscous damping factor
ζ_d, ζ_f	= see Eqs. (5), (6), respectively
θ_n	= body pitch in nth normalized mode shape
Θ	= pitch angle in absence of flexibility
θ, ϕ, ψ	= body pitch, roll, yaw angles
ω_n	= natural frequencies of entire spacecraft
Ω	= frequency of excitation
$(\ )_n$	= pertaining to nth vibration mode
$(\dot{\ })$	= differentiation with respect to time
$(\bar{\ })$	= Laplace transform

Received May 8, 1978; revision received Oct. 26, 1978.

Index categories: Spacecraft Dynamics and Control; Spacecraft Testing, Flight and Ground.

*Research Associate, Institute for Aerospace Studies. Member AIAA.
†Professor, Institute for Aerospace Studies. Member AIAA.
‡Research Engineer, Communications Research Centre.
§Research Scientist, Communications Research Centre. Member AIAA.

Introduction

THE Hermes spacecraft (alias Communications Technology Satellite) was inserted into geostationary orbit in Janurary 1976. The evaluation and testing of structural dynamics aspects of Hermes were part of an experimental program described in Ref. 1. Of particular interest is an experiment,[2] aimed at eliciting significant dynamics data in-flight by active excitation of the dominant vibration modes.[3] The design and results of this experiment are described in the present paper along with data from array deployment, slew transients, and prelaunch dynamics tests. The experimental frequencies, damping factors, and gains are compared with predictions from the authors' analytical model.

The Hermes spacecraft in its normal operating state, with both arrays deployed, is depicted in Fig. 1. The basic elements

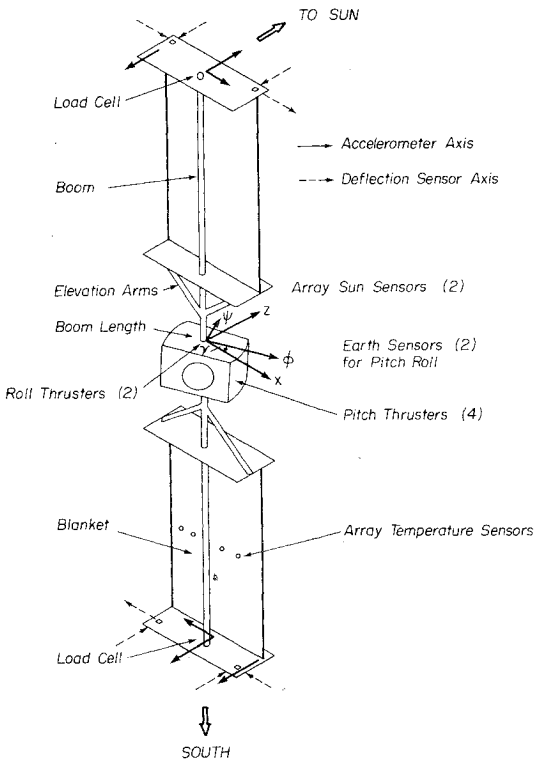

Fig. 1 Hermes spacecraft and instrumentation in deployed state.

of the attitude control system are also shown. In addition, thrusters can be fired by ground command to provide control torques about the roll, pitch, yaw axes, and an east-west stationkeeping force. The solar arrays face the Sun, the normal to the array plane making an angle γ with the yaw axis.

Three basic types of array deformation can be distinguished: twist (T) motion, in-plane (IP) bending, and out-of-plane (OP) bending. Due to symmetry in the spacecraft, these can be further grouped into symmetric and antisymmetric classes. Only symmetric twist, antisymmetric in-plane, and antisymmetric out-of-plane deformations interact with rotations of the center body. Their modal characteristics are important for attitude control system design.

Dynamical Models

The dynamics modeling for Hermes has evolved through a series of stages and has been aided by observations made in ground tests.[4] This evolution is qualitatively summarized in Ref. 5. A more detailed summary of the analysis, parameter values, and numerical results is given in Ref. 3, with references to original sources.[6] Figure 2 depicts the interaction between deformations, attitude dynamics of the center body, and applied torques and forces. Minor couplings are shown by dotted lines. From Fig. 1, it appears that OP bending interacts with the rotation δ about the x axis, and IP bending interacts with rotations ϵ about the z axis. The input torques T_1, T_2, etc., shown uncoupled in Fig. 2, are in fact slightly coupled due to geometrical misalignments. Furthermore, thrusters always cause a force concomitant to a torque, i.e., pure couples cannot be applied.

A single-axis example serves to illustrate the dynamical model. The pitch/twist dynamics can be expressed as follows, neglecting small couplings with other modes:

$$v(x,y,t) = -x\sum_{n=1}^{\infty}\alpha_n(y)q_n(t) \tag{1a}$$

$$\ddot{q}_n + \omega_n{}^2 q_n + [2\zeta_n\omega_n\dot{q}_n] = h_n\ddot{\Theta}(t) \tag{1b}$$

$$\theta = \Theta + \Sigma\theta_n q_n \qquad \ddot{\Theta} = T_2(t)/I_2 \tag{1c}$$

Attention is drawn to the "equivalent viscous damping factor" ζ_n. Its significance is purely empirical; it is inserted after $\{\omega_n,\ \theta_n,\ \alpha_n(y)\}$ have been calculated with energy dissipation neglected. Of further interest here are two transfer functions:

Between applied torque and attitude—

$$I_2 s^2\bar{\theta}(s) = \left[1 + \sum_{n=1}^{\infty}\frac{s^2 k_n}{s^2 + 2\zeta_n\omega_n s + \omega_n{}^2}\right]\bar{T}_2(s) \tag{2}$$

Between applied torque and acceleration at a point (x,y) on the blanket—

$$\bar{a}(x,y,s) = -x\left[1 + \sum_{n=1}^{\infty}\frac{s^2 d_n(y)}{s^2 + 2\zeta_n\omega_n s + \omega_n{}^2}\right]\frac{\bar{T}_2(s)}{I_2} \tag{3}$$

$$d_n = k_n[1 + \alpha_n(y)/\theta_n] \tag{4}$$

The acceleration gains d_n are products of the attitude gains k_n and a factor containing the normalized mode shapes. Similar transfer functions can be written for other single-axis situations, such as δ/OP bending interaction. To the order of experimental accuracy, one can neglect small couplings between modes due to geometric and kinematic offsets, asymmetries between north and south arrays, roll-yaw products of inertia, and roll-yaw coupling due to the momentum wheel.[3]

Numerical values for analytical predictions are now given. Natural frequencies, gains, and mode shapes were found by continuum-mechanics methods. The mass/stiffness parameters of the spacecraft given in Ref. 3 (Table 2.3) were used, except that 1) boom root stiffnesses have the values $k_1 = k_1' = 1000$ ft-lb$_f$, and 2) the boom bending stiffness values used there have been changed, in light of the test results reported in Ref. 7, to $B = 2480$, $B' = 2960$ lb$_f$-ft^2. The methods stated in Ref. 3 then lead to the natural frequencies ω_n listed in Table 1. Some acceleration gains d_n corresponding to the location of accelerometers (Fig. 1) are given later in Table 5. An adequate theory for the prediction of ζ_n does not exist. However, semiempirical methods can be devised for estimating ζ_n in space, given the appendage damping factors in space[6] or in the 1-g field on the ground.[8] These methods are highly approximate at best. Appendage damping factors were measured in ground tests of the Hermes solar arrays,[5] and Table 2 lists the best estimates of flight damping factors based on these results.

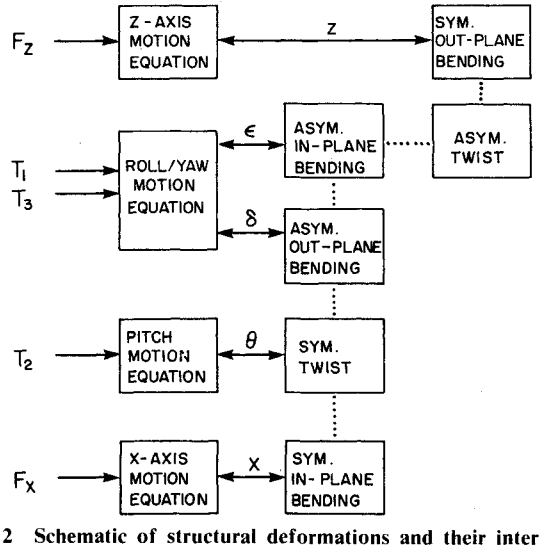

Fig. 2 Schematic of structural deformations and their interaction with attitude control.

Sources and Processing of Data

The most effective, convenient and operationally flexible means of excitation are the thrusters. Their output for commanded pulse widths greater than about 0.1 s may be idealized as a rectangular torque pulse, although a more detailed model is available.[3]

The sensors available for dynamics-related measurements are shown in Fig. 1, as well as approximate locations of the thrusters relevant here. The sampling frequency, digitization step size, and accuracy of selected sensors are given in Table 3. The measurements are transmitted by the telemetry, tracking, and command (TT & C) subsystem, which also

Table 1 Natural frequencies

Mode type	Predicted, Hz	Incidental exc., Hz	Special exc., Hz
Asym. OP-1	0.434	0.45	0.44
Asym. OP-2	0.504	. . .	0.50
Sym. OP-1	0.151	0.15	0.15
Asym. IP-1	0.793	0.76	0.88
Asym. IP-1 ($\gamma = 90$ deg)	0.886	. . .	0.98
Asym. IP-2	0.925	0.89	. . .
Sym. IP-1	0.278	0.30	0.31
Sym. T-1	0.171	0.20	0.17
Sym. T-2	0.508	0.46	. . .

Table 2 Damping factors

Mode type	Predicted[a] range	Incidental ζ_f	Incidental ζ_d	Spex results ζ_f	Spex results ζ_d
Asym. OP-1	0.005-0.009	0.015	0.018	0.022	0.020
Asym. OP-2	. . .	. . .	. . .	0.008	0.007
Sym. OP-1	0.003-0.006	0.038	0.033	0.03	. . .
Asym. IP-1	. . .	0.012	. . .	0.016	0.015
Sym. IP-1	0.014-0.02	0.039	0.035	0.03	. . .
Sym. T-1	0.09 -0.16	0.08	0.09	. . .	. . .

[a] Extrapolation of ground test results.

Table 3 Sensor characteristics

Measurement	Sampling rate, Hz	Quantization[a]	Accuracy[b]	Range
Roll angle, deg	1	0.011	0.017	±2.8
Pitch angle, deg (cross-scan axis)	1	0.013	0.017	±3.3
Boom compression, lb_f	1	0.06	0.5	0-32
Accelerations, milli-g:				
Boom tip (OP)	3	0.18-0.36	0.32	±97
Array edge (IP)	4	0.12	0.32	±97
Array corner (OP + T)	5	0.11	0.32	±97

[a] For nonlinear sensors, linearized in operating range.
[b] Expected error (1σ) in single measurement.

handles ground commands and provides command verification capability.

The six accelerometers used for structural dynamics measurements were located at the array ends as shown in Fig. 1. Four Systron-Donner type 4310F and two type 4310A accelerometers were used. Sample rates were selected to be in excess of twice the maximum expected dominant frequency of interest. Analog four-pole Butterworth filters with a 1-Hz cutoff were used before sampling to prevent aliasing errors. To accommodate the 8-bit spacecraft telemetry word length, while achieving suitable dynamic range, a combination of a maximum range of ±100 milli-g and a nonlinear gain circuit with high gain in the 0 to ±20 milli-g range was used. The resulting least-significant-bit-quantization varied from 0.18 milli-g at low amplitudes to 1.2 milli-g near the maximum range.

The largest accelerations actually measured in flight were about 15 milli-g, rendering the nonlinear gain circuit unnecessary. Similarly, the dominant IP frequency was high enough to be attenuated by the filters, so that a higher cutoff would have helped. However, the advantages of having filters were clearly established by the quality of data obtained.

Flight data in the telemetered bit stream were first transformed into engineering units, using prelaunch calibration curves. This was followed by inspection of data in selected time intervals. The accelerometer outputs, being linear combinations of six classes of modes, were processed to yield modal accelerations. Different sampling rates and minor timing differences were dealt with by Lagrange interpolation of measurements to construct synchronized samples at 4 Hz.

Typically, accelerometer outputs showed high signal-to-noise ratios, making stochastic estimation methods unnecessary. In many cases, only one mode was excited. Natural frequencies were obtained from the free response following an excitation, and confirmed by Fourier tranforms of modal accelerations, taking data over several overlapping time intervals.

The rate of decay of the free response of a single mode provides a measure of damping. Assuming a linear viscous model, the peak amplitudes yield ζ by the log decrement formula:

$$\zeta_d \equiv \frac{\zeta}{\sqrt{1-\zeta^2}} = -\frac{1}{2\pi(n-m)} \ell n\left(\frac{A_n}{A_m}\right) \qquad (5)$$

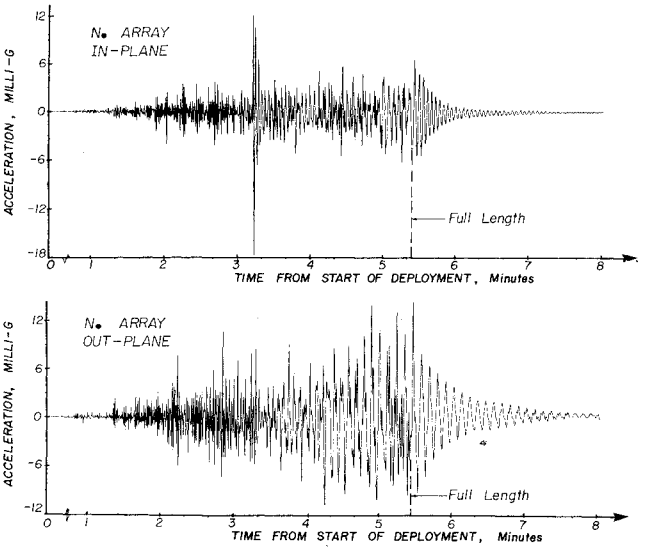

Fig. 3 Flight accelerations observed during deployment of solar arrays.

In practice, this value will depend on the peak numbers (m,n) chosen, due to the nonlinear, nonviscous nature of the damping, the response of additional flexible modes, and discretization errors. A better estimate of ζ_d is obtained by taking the mean for various (m,n). The peaks are indicated in a record of accelerations by points where the first differences change sign.

Another estimate for ζ is obtained in the frequency domain. The Fourier transform of a single damped sinusoid exhibits a resonance peak of width

$$\zeta_f = (\omega_2 - \omega_1)/(2\omega_n) \qquad (6)$$

where ω_2, ω_1 are frequencies where the magnitude of the tranform is $1/\sqrt{2}$ of its peak value. Unlike Eq. (5), this method can also handle more than one mode, if sufficiently separated in frequency. Although viscous damping estimates are inherently inexact, they do permit one to predict resonant amplitude, an important function of a dampling model.

Unlike ω_n and ζ, gains must be found from the response to a known input. One can obtain the acceleration gains of Eq.

(3) from accelerometer outputs, but not the attitude gains k_n, due to poor resolution of attitude data. The estimation of gains is inextricably linked with that of dampling factors ζ, for which an independent value is available from the free response. Knowing ζ and the theoretical gains, one can predict the resonant steady-state amplitudes.

Incidental Excitation

By design, the normal attitude control torques do not measurably excite structural vibrations, but significant vibrations occurred during initial array deployment on day 32, 1976, and during a large-angle array slew following temporary loss of attitude control on day 273, 1976.

During inital deployment, the north and south arrays deployed at somewhat different rates. Relatively large symmetric IP/OP bending and antisymmetric twisting accelerations were observed. Figure 3 shows the north out-of-plane and in-plane accelerations. The portion following attainment of full length is indicative of the on-orbit dynamics. For twist and symmetric bending, the dominant natural frequencies were readily located in Fourier transform plots. Damping estimates ζ_d, ζ_f were obtained as discussed earlier. The results for $\zeta_d(n,m)$ became erratic for large n,m (when amplitudes become small) indicating that the viscous approximation is not valid for very small deformations.

The observed frequencies and damping in postdeployment data are given in Tables 1 and 2, respectively. Partial confirmation of frequencies was obtained from array slew data, but damping could not be reliably estimated, due to low amplitudes. The twist damping value in Table 2 is similarly unreliable. Comparison of results with predicted values (Table 1) shows good agreement for bending frequencies. The estimates from the array slewing and postdeployment data agree despite a 240-day period between the two, indicating that repeated eclipses and the general space enviroment have negligible effect on spacecraft dynamic characteristics.

Special Excitation

The Special Excitation (Spex) experiment can be viewed as a vibration test in space. However, it is not possible to leisurely sweep through a range of input frequencies (due to limitations on spacecraft time available), and stringent restrictions on spacecraft structural response and on complexity of operating procedures are necessary to minimize risk to the mission.

Near-resonant testing is the preferred method for this problem.[3] Its advantages are 1) direct isolation and pinpointing of resonant frequencies, 2) larger amplitudes, yielding high signal-to-noise ratios and damping over a range of amplitudes, 3) simplification of analysis, design, and simulation, and 4) more reliable interpretation of results. The chief limitations are the inherent restriction to one mode at a time, and the critical dependence of resonant amplitudes on damping (for $\zeta \ll 1$), which is amplitude-dependent and poorly known in advance.

The basic input for exciting resonance is shown in Fig. 4 and can be implemented by alternating thruster firings. A Fourier series expansion of this input is (assuming an infinite pulse train)

$$f(t) = \sum_{m=-\infty}^{\infty} c_m e^{im\Omega t} \tag{7}$$

$$c_m = \frac{iA}{m\Omega t}\left(1 - e^{-im\Omega T_1}\right)\left(e^{-im\Omega\Delta} - 1\right) \tag{8}$$

Setting $T_1 = T/2$, where $T = 2\pi/\Omega$ is the period,

$$|c_m| = \frac{2A}{m\pi}\left|\sin\left(\frac{m\Omega\Delta}{2}\right)\right| \quad (m \text{ odd})$$
$$= 0 \quad (m \text{ even}) \tag{9}$$

Resonance occurs when the dominant term in this expansion ($m = 1$) coincides with some ω_n in the transfer functions of Eq. (3). Usually, we wish to excite the first spacecraft mode. Different mode types require different thrusters, e.g., roll thrusters will excite antisymmetric OP bending ($\gamma = 0$ deg, 180 deg) and antisymmetric IP bending ($\gamma = 90$ deg, 270 deg).

For low damping, the spacecraft response during Spex is determined largely by the resonant term in the transfer function, barring multiple resonances. The steady-state resonant amplitude for the first mode in Eq. (3) is

$$a_{\max.} \doteq \frac{4Fl}{I_2\pi}\left|\sin\frac{\Omega\Delta}{2}\right|\left[\left[\frac{x_a d_1(y_a)\Omega^2}{|(\omega_1^2 - \Omega^2) + 2i\zeta\omega_1\Omega|}\right]\right] \tag{10}$$

$$d_1(y_a) \equiv k_1[1 + \alpha(y_a)/\theta_1] \tag{11}$$

where (x_a, y_a) is the accelerometer location. Similar expressions apply to other mode types. The one-mode approximation is reasonable, as shown by simulation.[3]

Designing the input consists of choosing the frequency Ω and pulse width Δ. It is desirable to make Ω as close as possible to the target frequency ω_1. The width Δ is chosen based on the maximum resonant amplitude, predicted by Eq. (10). This presupposes good knowledge of the gain d_1 and ζ, but the latter is poorly known. A detailed treatment of the resonant experiment design is given in Ref. 3, including numerical results from detailed simulations.

Preliminary Excitation

Excitation to resonance is very sensitive to ζ. Measurable accelerations may not be excited if Ω differs from ω_1 by even 5%. A preliminary experiment was thus aimed at estimating ζ and ω_1, and at demonstrating the safety of the excitation procedure. Its design must be relatively insensitive to ζ, and must give good results for modal frequencies ω_1 at least in the range ($\Omega \pm 10\%$). These properties are not achievable by single-frequency resonant excitation, but may be obtained from considerations of transient response.

The response of an initially quiescent, linear stationary system can be written as

$$y(t) = \int_0^t w(t-\tau)u(\tau)\,d\tau \tag{12}$$

A graphic interpretation of this is shown in Fig. 4, where the impulse response w is representative of a single flexible mode:

$$w(s) = -\frac{e^{-\zeta\omega_1 s}}{\sqrt{1-\zeta^2}}\sin\omega_1\sqrt{1-\zeta^2}\,s \tag{13}$$

for $\zeta = 0.02$. For low damping ($\zeta \ll 1$), it is clear that the response for small T, i.e., for a small number of pulses, is not critically dependent on ζ. Figure 4 also shows that the largest response is obtained when $u(\tau)$ is "in phase" with $w(t-\tau)$. The effect of a mismatch in frequency, $|\Omega - \omega_1|$, is to produce

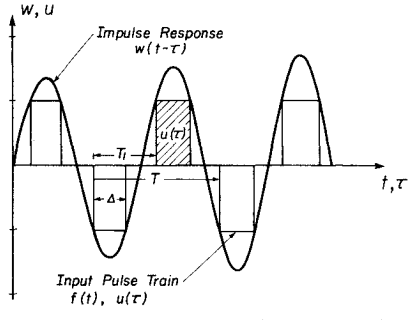

Fig. 4 Excitation input and graphical illustration of impulse response.

a progressively increasing phase shift between $u(\tau)$ and $w(t-\tau)$. The maximum phase shift for N pulses is

$$\phi_N = \omega_l |N\pi/\omega_l - N\pi/\Omega| \tag{14}$$

The largest tolerable value for this is $\phi_N = \pi$, when the last pulse is opposite in polarity to that dictated by w. For an uncertainty in ω_n of $(\Omega \pm 10\%)$, this criterion gives $N = 10$. This design of the preliminary excitation has the additional virtue that its implementation is identical to that of resonant excitation.

A complete Spex experiment for a given mode type consists of three sets of thruster firings, termed the A, B, and C "burns," respectively. The first two are preliminary excitations and the third is a resonant excitation to steady state, with Ω and Δ chosen on the basis of (ω_l, ζ) obtained in the A and B burns. The thruster firing commands are sent to the spacecraft under software control. Roll thrusters were used due to previous operating experience. Preparation for an experiment included waiting for the appropriate orbit slot (value of γ); turning on and off the requisite sensors, telemetry encoders, thruster valves, and heaters, etc.; and disabling the attitude control system and array tracking for the duration of the experiment. This was carried out with the support of spacecraft systems engineers and operations personnel.

Results

The several burns conducted in the Spex experiment had characteristics summarized in Table 4. The IP-A′ burn was a repetition of IP-A 12 h (180-deg in γ) later, to assess the effect of γ on mass-center offsets, and showed that offsets were negligible near $\gamma = 0$ and 180 deg. Table 4 shows that attitude excursions were quite modest. The safety bounds on response were all met: attitude (roll <0.5 deg, pitch <0.4 deg), deflections (<4 in.), and accelerations (<9 milli-g). The largest disturbances occurred during the resonant C burns. The experiments were very satisfactory in terms of both the quality and quantity of data obtained.

Accelerations measured during the IP-C burn are shown in Fig. 5. The qualitative behavior of damping seen in Fig. 5a may be classified into three phases: first a rapid viscous-like exponential decay, a low-amplitude termimal region exhibiting a linear envelope characteristic of Coulomb damping, and a transition region in between. Not explicitly shown in Fig. 5a is the fact that north and south array

Table 4 Special excitation firings

Burn type	Period, s	Width, s	Roll peak, deg	Pitch peak, deg
OP-A	2.22	0.28	±0.06	0.03
OP-B	2.16	0.47	±0.11	[a]
OP-C	2.14	0.48	±0.15	−0.08
IP-A	1.20	0.17	[a]	−0.11
IP-B	1.06	0.29	[a]	−0.18
IP-A′	1.06	0.17	±0.03	0.13
IP-C	1.04	0.14	±0.03	0.34

[a] Negligible deviation from normal operation.

Table 5 Amplitudes and gains

Quantity	Antisymmetric OP bending	Antisymmetric IP bending
Predicted maximum amplitude, milli g	8.01	3.82
Corrected for number of pulses	6.98	2.97
Corrected for filter gain	6.98	1.67
Observed amplitude	6.6	1.6
Acceleration gain inferred	1.28	1.26
Acceleration gain predicted	1.35	1.29

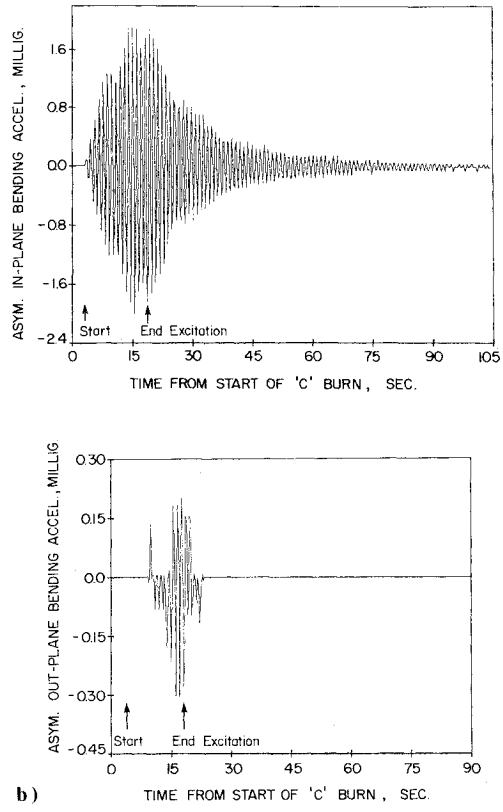

Fig. 5 Processed flight accelerations, observed during IP-C burn excitation: a) antisymmetric IP bending, b) antisymmetric OP bending.

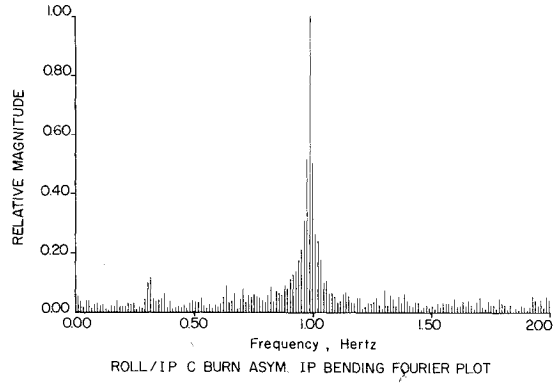

Fig. 6 Fourier transform of observed in-plane accelerations.

responses were very similar, i.e., a true antisymmetric mode was excited. This is also indicated by the very small OP bending response in Fig. 5b. Figure 6 shows the Fourier transform of the free response in Fig. 5a. It is clear that virtually a single mode was excited in the IP-C burn. The results for A and B burns were similar.

Figure 7 shows the antisymmetric OP bending and symmetric twisting accelerations during the OP-C burn. The significant coupling observed can be qualitatively traced to an in-plane offset of the tip pallet mass center with respect to the boom. A "beating" phenomenon is evident; it was present in the OP-A and OP-B burns also. The explanation for this was variously sought in north/south asymmetries and in coupling with twisting or symmetric OP bending modes. However, the combined evidence of several time and Fourier transform plots is that two antisymmetric bending frequencies are indeed adjacent, the response of the second mode being accentuated by much lower damping. The beating masks the regions of damping found in the IP case, but it is clear that smaller

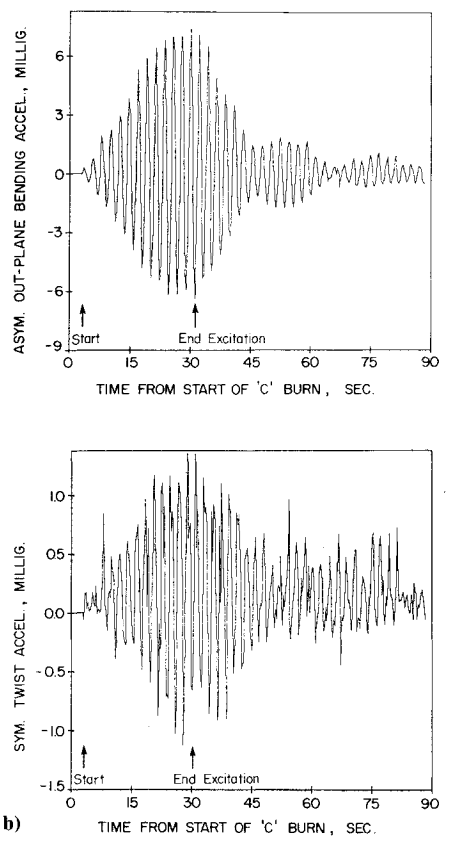

Fig. 7 Processed flight accelerations, observed during OP-C burn excitation: a) antisymmetric OP bending, b) symmetric twist.

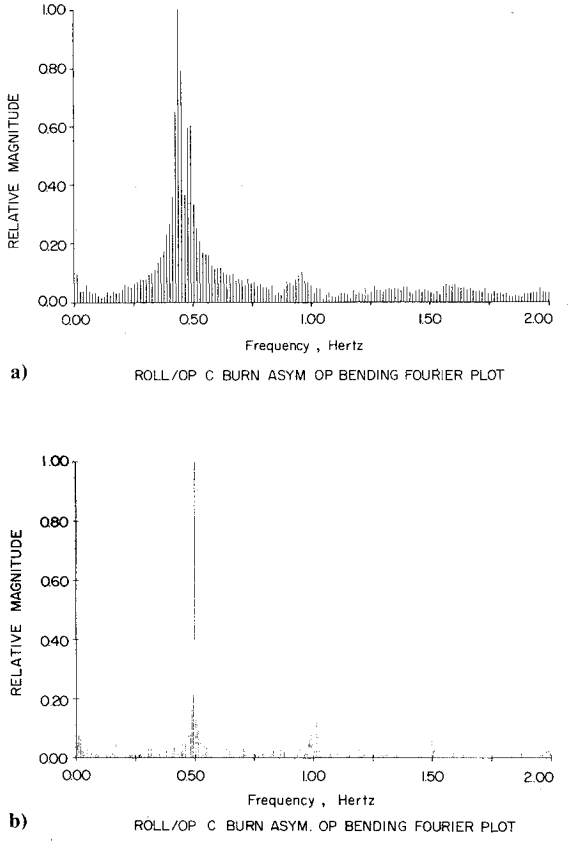

Fig. 8 Fourier transforms of observed out-of-plane accelerations: a) normal free response, b) low-amplitude residual response.

amplitudes decay more slowly. Not shown in Fig. 7 are marked differences in response of the two arrays, with north showing a persistent low-amplitude oscillation long after south had subsided. The reason for this has not been conclusively established.

Fourier transforms of the OP-C bending response are shown in Fig. 8. The two adjacent antisymmetric OP frequencies are clearly seen. The second mode appears to be more lightly damped. Figure 8b shows the Fourier plot for the antisymmetric OP bending response remaining after larger amplitudes have subsided. A highly underdamped peak is found, corresponding to the second mode which has very low damping ($\zeta \approx 0.008$). Fourier transform methods were also able to detect small differences, predicted by theory, between frequencies at $\gamma = 0$ and 90 deg.

The values of frequencies inferred from Spex compare well with predictions and incidental results, as seen in Table 1. Damping factors are compared in Table 2. Excellent agreement is observed overall with theoretical values in Table 1. It is also noteworthy that consistent estimates of ζ are obtained by both Fourier-transform and averaged log-decrement methods.

Comparison of amplitudes is also of interest. With the theoretical values for d_l and empirical values of ζ, Eq. (10) predicts the ideal resonant amplitude, which must be corrected for the finite number of pulses and for attenuation by the filters. The first correction is applied assuming a $(1 - e^{-\zeta\omega t})$ envelope. The second is based on steady-state attenuation from the filter frequency response, and is significant (−5 dB) only at IP bending frequencies. Table 5 compares the ideal and corrected predictions with observed amplitudes in the IP-C and OP-C burns. Excellent agreement is seen. Although empirical values of ζ were used in the prediction, these are known to be representative of large (resonant) amplitudes. The comparison is thus a valid test of gains, which are also compared in Table 5.

Theory vs Experiment

The measured frequencies compare favorably with theory, as seen from the comparative data in Table 1. All modes except IP bending show agreement within 1%. The IP predictions fall below experimental values by about 10%. The analytical model for IP bending is relatively inaccurate, because 1) the array under tension is assumed rigid except for the boom, 2) a large part of IP stiffness is provided by the elevation arms, modeled as an effective spring constant k_2, and 3) k_2 and the boom root stiffness k_1' are poorly known (not a fault of the model). By increasing k_2 and k_1' from their nominal values, better agreement of IP frequencies can be obtained. The agreement of twist frequencies with theory is suprisingly good in view of the discrepancies noted in ground tests, and attributed to the nonuniform tension distribution in the blanket.[5]

The continuum-mechanics model is tractable and much simpler than elaborate finite-element models, but is seen to agree well with experiment. The number of well-predicted modes is large and in one case (OP) the second mode is also predicted well, so that the good agreement is not a chance occurrence. The model is further confirmed by the agreement between amplitudes in Table 5. Although gains are bounded by the ratio of flexible to rigid inertia,[6] acceleration gains depend on the mode shapes, which are not well predicted by theory. Considering this and the critical dependence on ζ, the amplitude comparison appears even more favorable.

Estimates of damping using frequency-domain methods agree well with the mean of conventional log-decrement estimates. The damping factors measured in space are substantially higher than expected from structural energy dissipation, and higher also than estimates derived from ground test results. This emphasizes the difficulty of damping prediction. Damping is quite high in twist, probably due to the rubbing of two layers in the BISTEM boom, and is higher in symmetric bending than in antisymmetric. The damping

factor apparently increases with lower frequency, which suggests frequency-sensitive, nonlinear sources of energy dissipation. Dissipation exists in the boom actuator, array Sun-tracking motor, folds and hinges in the blanket, the elevation arms, the boom cross section, and in propellant tanks; but insufficient data exist to trace modal damping factors to these various causes. Hence, it is not clear how these damping values should be extrapolated to other spacecraft.

Concluding Remarks

The Hermes dynamics experiments have shown that for this class of spacecraft, continuum-mechanics modeling is tractable, accurate, and convenient. The well-known advantages of this classical method include a considerable saving in analysis and computation costs.[4]

The importance of damping factors makes the discrepancy between expectations and observed values an area of concern. Unfortunately, advances in theoretical prediction of dissipation for a complex spacecraft do not look promising. An attractive solution on future spacecraft is to put in artifical, viscous dampers designed for the dominant modes, assuming the availability of a workable mechanical device for the low frequencies and amplitudes of concern.

The relative simplicity of the preliminary excitation and its success in establishing (ω_n, ζ) make it attractive. If accelerometers are present—and it is to be hoped that on a flexible spacecraft they would be—this type of experiment can be conducted without appreciable risk to the mission. The spacecraft parameters thus obtained could be used to adjust parameters in the attitude control system, by ground command or automatically.

The authors feel that a relatively complete picture of Hermes dynamics in space has been obtained by fairly modest instrumentation and that the advantages of instrumenting a flexible spacecraft for dynamics measurements have been established.

Acknowledgments

The first two authors' work was supported by the National Research Council of Canada under grant S-7309. The experiments described here required close cooperation between many individuals from five separate organizations: University of Toronto, Communications Research Centre, Spar Aerospace Limited, SED Systems Limited, and NASA Lewis Research Center. Special thanks are due N.A. Harrison and H.R. Raine of the Communications Research Centre, and E.A. McPherson of SED Systems Limited.

References

[1] Vigneron, F.R. and Millar, R.A., "Plan for Flight Evaluation of Attitude Stabilization and Flexible Solar Array Dynamics for the Communications Technology Satellite," presented at International Astronomical Federation (IAF), 26th Congress, Lisbon, Portugal, Sept. 21-27, 1975.

[2] Hughes, P.C., "Design of an In-Orbit Dynamics Experiment for System Identification and Estimation," *Lecture Notes, Lectures on the Dynamics and Control for Nonrigid Spacecraft,* European Research Organization, ESTEC, Noordwijk, The Netherlands, June 1975.

[3] Garg, S.C., "Near-Resonant Vibration Tests of an Orbiting Flexible Spacecraft: Theory, Design and Simulation," Univ. of Toronto, Institute for Aerospace Studies, Toronto, Canada, UTIAS Rept. 204, Nov. 1976.

[4] Harrison, T.D., "Functional and Dynamics Testing of the Flexible Solar Array for the Communications Technology Satellite," Paper No. 24, 8th Conference on Space Simulation, NASA SP-379, 1975.

[5] Vigneron, F.R. and Hughes, P.C., "Structural Dynamics for Hermes—Modelling and Measurements," *Hermes—Its Performance and Applications,* Royal Society of Canada Symposium, Ottawa, Nov. 29-Dec. 1, 1977.

[6] Hughes, P.C., "A Model for the Attitude Dynamics of CTS with Reference to Attitude Control System Design," Aerospace Engineering and Research Consultants Ltd., Downsview, Ont., AERCOL Rept. No. 75-14-4, 1975.

[7] Gossain, D.M., "Results of Tests on CTS Flight Actuator to Determine Boom Root Backlash," Spar Aerospace Products Ltd., Toronto, Canada, TM 1142, Jan. 1975.

[8] Vigneron, F.R., "Ground-Test Derived and Flight Values of Damping for a Flexible Spacecraft," European Space Agency, ESA-SP-117, May 1977, pp. 325-333.